Letters

An LCCC-LCC Compensated Dual-Coupled WPT System With MI Enhancement and High Misalignment Tolerance

Jing Feng, Guo Wei, Jiantao Zhang, and Chunbo Zhu, *Member, IEEE*

***Abstract*—In this letter, an *LCCC-LCC* compensated dual-coupled wireless power transfer system is proposed to enhance the mutual inductance (MI) and antimisalignment capability. Only one capacitor is added to the *LCC*-compensated primary side. Not only the similar transfer characteristic to that of the *LCC-LCC* compensated system, like the load independent constant current output with zero phase angle (ZPA), but also the enhanced stable equivalent MI can be flexibly designed by introducing the MI adjustment factor λ. Thus, a stable output is efficiently offered. A 3.3-kW experimental prototype with Al plate is designed for validation. The result shows that the fluctuation of the load current is 5% within the 120 mm misalignment and the dc–dc efficiency of the system can be maintained above 90%.**

***Index Terms*—Compensation topology design, dual-coupled system, misalignment tolerance, mutual inductance enhancement, wireless power transfer.**

I. Introduction

WIRELESS power transfer (WPT) topology has received considerable attention due to its convenience and flexibility [1]. Despite having the advantages, coil misalignment is an inherent problem of the WPT system. The system works well only when coils are reasonably well aligned, which is not normally available in most practical applications. Therefore, it is vital to strengthen the antioffset capability of WPT systems and several methods have been proposed, such as the following.

1) Some control schemes like single-variable control and multivariable control are presented [2], [3], [4]. These approaches are generally assisted with the communication mechanism and the complicated control circuit and also suffer from the large modulation index.

Manuscript received 3 August 2023; revised 4 September 2023; accepted 21 September 2023. Date of publication 25 September 2023; date of current version 23 October 2023. This work was supported in part by the National Natural Science Foundation of China under Grant 51577041 and Grant 51811530102. *(Corresponding authors: Guo Wei; Jiantao Zhang.)*

Jing Feng and Guo Wei are with the School of Electrical Engineering and Automation, Harbin Institute of Technology, Harbin 150001, China, and also with Harbin Institute of Technology, Zhengzhou Research Institute, Zhengzhou 450000, China (e-mail: hitjingfeng@stu.hit.edu.cn; hitweiguo@hit.edu.cn).

Jiantao Zhang and Chunbo Zhu are with the School of Electrical Engineering and Automation, Harbin Institute of Technology, Harbin 150001, China (e-mail: jiantaoz@hit.edu.cn; zhuchunbo@hit.edu.cn).

Color versions of one or more figures in this article are available at https://doi.org/10.1109/TPEL.2023.3319023.

Digital Object Identifier 10.1109/TPEL.2023.3319023

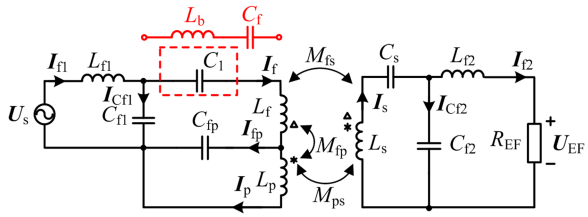

Fig. 1. Equivalent circuit of the proposed *LCCC-LCC* compensated dual-coupled WPT system.

2) Compared with the control strategy, the inherent capability of the magnetic coupling mechanism against misalignment is the preferred approach. A simple approach is to add the antiseries coils to the normal coil and a nearly constant mutual inductance (MI) between the primary and secondary coils is created by using the flux cancellation. In [5], the antiseries coil is first employed in the primary coil to improve the misalignment tolerance. Thereafter, a series of research have been reported, which includes the antiseries transmitting coil, the antiseries receiving coil, and multiple antiseries coils [6], [7], [8]. In the above-mentioned studies, MI(s) between different coils should have the same variation trend to guarantee a constant value of MI(s) subtraction. Resultantly, the coil structures and parameters are restricted.
3) As alternative methods, the compensation topology design, including the reconfigurable topologies [9], [10] and the hybrid compensation topology [11], [12] can be used to stabilize the output against the misalignment. However, the switching control is generally required in reconfigurable systems. This means that the system should be equipped with a precise detection module and control circuit, even with real-time communication, which will burden the system. In the hybrid compensation system, to suppress cross coupling, the coil structure is usually constrained and Double D, Bipolar, and Double D Quadrature are the preferred choices. As a result, the misalignment tolerance is limited.

In this letter, an *LCCC-LCC* compensated dual-coupled WPT system is proposed. Compared with the *LCC-LCC* system, only one capacitor is added to the primary side. The relationship of compensation parameters, the equivalent MI value, and the MI

variation characteristics of the dual-coupled coil is inherently established by introducing MI adjustment factor λ. The calculation method of λ is also provided based on the relationship between the MI(s) variation curves of the dual-coupled coils. In this way, the enhanced stable equivalent MI can be flexibly designed, including its value and fluctuation, and thus, a stable efficient output is obtained.

II. Modeling and Analysis

A. Equivalent Circuit Analysis

The equivalent circuit of the proposed system is shown in Fig. 1. The subcoils $L_{\rm f}$ and $L_{\rm p}$ are reversely connected in series as the transmitting coil and the mutual inductances between coils $L_{\rm f}$, $L_{\rm p}$, and $L_{\rm s}$ are $M_{\rm fp}$, $M_{\rm fs}$, and $M_{\rm ps}$, respectively. $L_{\rm f1}$ and $L_{\rm f2}$ are the compensation inductors of the transmitting and receiving coils. $C_{\rm f1}$, $C_{\rm f2}$, C_1, $C_{\rm s}$, and $C_{\rm fp}$ are the compensation capacitors. For easy analysis, the capacitor C_1 is split into the inductor $L_{\rm b}$ and the capacitor $C_{\rm f}$. Coils $L_{\rm f1}$ and $L_{\rm b}$, and the capacitor $C_{\rm f1}$ constitute the T-circuit. Parameters satisfy

$$\begin{cases} 1/(\mathrm{j}\omega C_1) = \mathrm{j}\omega L_{\rm b} + 1/(\mathrm{j}\omega C_{\rm f}) \\ 1/(\mathrm{j}\omega C_{\rm f1}) = -\mathrm{j}\omega L_{\rm f1} = -\mathrm{j}\omega L_{\rm b} \end{cases} \tag{1}$$

where ω is the resonant frequency of the system.

The circuit equations are obtained based on Kirchhoff's law and expressed as

$$\begin{cases} (\mathrm{j}\omega L_{\rm f1} + 1/\mathrm{j}\omega C_{\rm f1})\,\boldsymbol{I}_{\rm f1} - 1/\mathrm{j}\omega C_{\rm f1}\boldsymbol{I}_{\rm f} - \boldsymbol{U}_{\rm s} = 0 \\ \left(\mathrm{j}\omega L_{\rm b} + Z_{\rm Lfe} + Z_{\rm Ce} + 1/\mathrm{j}\omega C_{\rm f1}\right)\boldsymbol{I}_{\rm f} - 1/\mathrm{j}\omega C_{\rm f1}\boldsymbol{I}_{\rm f1} \\ - Z_{\rm Ce}\boldsymbol{I}_{\rm p} + \mathrm{j}\omega M_{\rm fs}\boldsymbol{I}_{\rm s} = 0 \\ - Z_{\rm Ce}\boldsymbol{I}_{\rm f} + (Z_{\rm Ce} + Z_{\rm Lpe})\boldsymbol{I}_{\rm p} - \mathrm{j}\omega M_{\rm ps}\boldsymbol{I}_{\rm s} = 0 \\ \mathrm{j}\omega M_{\rm fs}\boldsymbol{I}_{\rm f} - \mathrm{j}\omega M_{\rm ps}\boldsymbol{I}_{\rm p} + (\mathrm{j}\omega L_{\rm s} + 1/\mathrm{j}\omega C_{\rm s} + 1/\mathrm{j}\omega C_{\rm f2})\boldsymbol{I}_{\rm s} \\ - 1/\mathrm{j}\omega C_{\rm f2}\boldsymbol{I}_{\rm f2} = 0 \\ - 1/\mathrm{j}\omega C_{\rm f2}\boldsymbol{I}_{\rm s} + (\mathrm{j}\omega L_{\rm f2} + 1/\mathrm{j}\omega C_{\rm f2})\,\boldsymbol{I}_{\rm f2} + \boldsymbol{U}_{\rm EF} = 0 \end{cases} \tag{2}$$

where

$$\begin{cases} Z_{\rm Lfe} = \mathrm{j}\omega L_{\rm fe} = \mathrm{j}\omega(L_{\rm f} - M_{\rm fp}) + 1/(\mathrm{j}\omega C_{\rm f}) \\ Z_{\rm Lpe} = \mathrm{j}\omega L_{\rm pe} = \mathrm{j}\omega\,(L_{\rm f} - M_{\rm fp}) \\ Z_{\rm Ce} = 1/(\mathrm{j}\omega C_{\rm e}) = \mathrm{j}\omega M_{\rm fp} + 1/(\mathrm{j}\omega C_{\rm fp})\,. \end{cases} \tag{3}$$

The parameter design of the secondary side is identical to that of the conventional *LCC* compensation and satisfy

$$\begin{cases} 1 - \omega^2 L_{\rm f2} C_{\rm f2} = 0 \\ 1 - \omega^2\,(L_{\rm s} - L_{\rm f2})\,C_{\rm s} = 0. \end{cases} \tag{4}$$

The input impedance $\boldsymbol{Z}_{\rm in}$ can be obtained when combined with (1)–(4) as

$$\boldsymbol{Z}_{\rm in} = \frac{\omega L_{\rm f1}}{R_{\rm EF}} \frac{(\omega L_{\rm f2})^2\left(\omega^2 L_{\rm pe} C_{\rm e} - 1\right) - \mathrm{j}\omega^3 M_{\rm ps}^2 C_{\rm e}}{\alpha + \mathrm{j}\beta} \tag{5}$$

where $\alpha = -(M_{\rm fs} + M_{\rm ps})^2\omega + \omega^3(M_{\rm ps}{}^2 L_{\rm fe} + M_{\rm fs}{}^2 L_{\rm pe})C_{\rm e}$ and $\beta = (\omega L_{\rm f2})^2\,[L_{\rm fe}(-1 + \omega^2 L_{\rm pe} C_{\rm e}) - L_{\rm pe}]/R_{\rm EF}$.

To achieve zero phase angle (ZPA) input, the input impedance of the system should be purely resistive. For WPT systems, MI is generally designed to be $0.1L_{\rm pe}$ to $0.3L_{\rm pe}$ ($0.1L_{\rm fe}$ to $0.3L_{\rm fe}$) and the equivalent load resistance of the battery is generally in the order of Ohm in the first charging stage [13]. Thus, the equivalent capacitor $C_{\rm e}$ can be approximately obtained as

$$C_{\rm e} = \frac{1+\lambda}{\lambda}\frac{1}{\omega^2 L_{\rm pe}} \tag{6}$$

where λ is the impedance ratio of $Z_{\rm Lfe}$ and $Z_{\rm Lpe}$, which is defined as the MI adjustment factor, and given by

$$\lambda = \frac{Z_{\rm Lfe}}{Z_{\rm Lpe}} = \frac{L_{\rm f} - M_{\rm fp} - 1/\left(\omega^2 C_{\rm f}\right)}{L_{\rm p} - M_{\rm fp}}. \tag{7}$$

Thus, the current can be obtained using (1)–(4), and (6) as

$$\begin{cases} \boldsymbol{I}_{\rm f1\_LCCC} = \mathrm{j}\frac{(M_{\rm fs}+\lambda M_{\rm ps})}{\omega L_{\rm f1} L_{\rm f2}}\boldsymbol{U}_{\rm EF}, \boldsymbol{I}_{\rm f2\_LCCC} = \frac{(M_{\rm fs}+\lambda M_{\rm ps})}{\mathrm{j}\omega L_{\rm f1} L_{\rm f2}}\boldsymbol{U}_{\rm s} \\ \boldsymbol{I}_{\rm f\_LCCC} = -\frac{\mathrm{j}\boldsymbol{U}_{\rm s}}{\omega L_{\rm f1}}, \boldsymbol{I}_{\rm p\_LCCC} = \frac{\mathrm{j}\lambda\boldsymbol{U}_{\rm s}}{\omega L_{\rm f1}}, \boldsymbol{I}_{\rm s\_LCCC} = \frac{\mathrm{j}\boldsymbol{U}_{\rm EF}}{\omega L_{\rm f2}}. \end{cases} \tag{8}$$

Define $M_{eq} = M_{fs} + \lambda M_{ps}$ (9)

is the equivalent MI of the proposed dual-coupled system.

B. Comparison of Proposed System and LCC System

For comparison, the current of the general *LCC-LCC* compensated system is given as [14]

$$\begin{cases} \boldsymbol{I}_{\rm f1\_LCC} = \mathrm{j}\frac{M_{\rm ps}}{\omega L_{\rm f1} L_{\rm f2}}\boldsymbol{U}_{\rm EF}, \boldsymbol{I}_{\rm f2\_LCC} = \frac{M_{\rm ps}}{\mathrm{j}\omega L_{\rm f1} L_{\rm f2}}\boldsymbol{U}_{\rm s} \\ \boldsymbol{I}_{\rm p\_LCC} = -\frac{\mathrm{j}\boldsymbol{U}_{\rm s}}{\omega L_{\rm f1}}, \boldsymbol{I}_{\rm s\_LCC} = \frac{\mathrm{j}\boldsymbol{U}_{\rm EF}}{\omega L_{\rm f2}}. \end{cases} \tag{10}$$

The phasor diagram of the ac currents and voltages of the proposed *LCCC-LCC* compensated system and the general *LCC-LCC* compensated system are shown in Fig. 2.

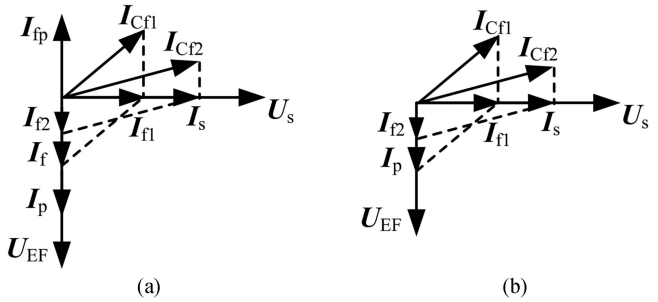

Fig. 2. Phasor diagram of the ac currents and voltages. (a) Proposed system. (b) *LCC-LCC* compensated system.

It can be seen from (8)–(10) and Fig. 2 that the proposed system shows similar transfer characteristics to that of the conventional *LCC* system. The relationship between the current phasor and the voltage phasor of the proposed system is the same as that of the general *LCC* system. The proposed design also offers a load-independent constant current (CC) output at ZPA, which can be an alternative to the *LCC-LCC* topology. Different from the *LCC-LCC* system, in which the output current $\boldsymbol{I}_{\rm f2\_LCC}$ is only related to ω, $M_{\rm ps}$, $L_{\rm f1}$, $L_{\rm f2}$, and $\boldsymbol{U}_{\rm s}$, it is clear that $\boldsymbol{I}_{\rm f2\_LCCC}$ of the proposed system is also dependent on the MI adjustment factor λ. In detail, $M_{\rm eq}$ and $\boldsymbol{I}_{\rm f2\_LCCC}$ can be flexibly adjusted with the help of the λ. The adjustment not only includes the value but also the fluctuation, which indicates that the antimisalignment capacity with the magnified $M_{\rm eq}$ can be obtained simultaneously. In addition, unlike the simple antiseries coil structure, it is not necessary to guarantee the identical

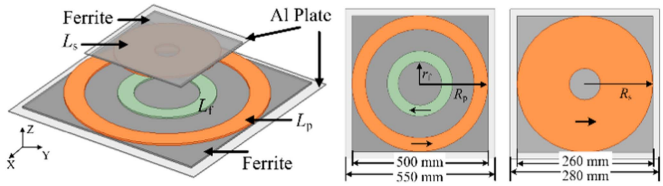

Fig. 3. Configuration of the coupling mechanism.

TABLE I
PARAMETERS OF COUPLING MECHANISM

Coil L_p		Coil L_f		Coil L_s	
R_p	N_p	r_f	N_f	R_s	N_s
250 mm	10	80 to 120 mm	8 to 15	130 mm	20

variation trend of the two MI(s) for a constant reduced value of $|M_{fs}$-$M_{ps}|$. The design of the coil structure is more flexible with the proposed method.

III. Design of High-Misalignment Tolerant Systems With Magnified Mutual Inductance

A. Adjustment Factor Analysis and Design for Stable Magnified MI

Recommended by SAE J2954 standard, the configuration and dimensions of the coupling mechanism are shown in Fig. 3 [15]. The related parameters are listed in Table I.

The relationship between *M*fs and *M*ps can be expressed by a linear function as [16]

$$M_{fs} = KM_{ps} + b \tag{11}$$

where K and b are the slope and intercept of the function.

M_{eq} can be calculated using (9) and (11) by

$$M_{eq} = (K + \lambda) M_{ps} + b. \tag{12}$$

To achieve M_{eq} independent of misalignment distance D_y, the following equation should be satisfied as:

$$\lambda = -K. \tag{13}$$

Therefore, the equivalent MI M_{eq} is expressed as

$$M_{eq} = b. \tag{14}$$

It can be seen from (13) and (14) that λ can be calculated by the ratio of the slope K. The equivalent MI is only related to b, which is constant and independent of D_y. Thus, a high anti-misalignment ability is achieved.

For different r_f and N_f, the relationship between M_{fs} and M_{ps}, and the calculated M_{eq} are given in Fig. 4. The transfer distance (AG) is 130 mm. As shown in Fig. 4(a-1), (b-1), and (c-1), the relationship between M_{fs} and M_{ps} can be approximately regarded as a linear function and the slope K becomes large with N_f increases. The minimum and maximum M_{eq}, and the corresponding MI fluctuation δ are marked in Fig. 4(a-2), (b-2), and (c-2). It can be seen that M_{eq} tends to be larger with the increase of N_f. Also, the variation of M_{eq} is very small and the fluctuation maintains about 5% in the whole misalignment

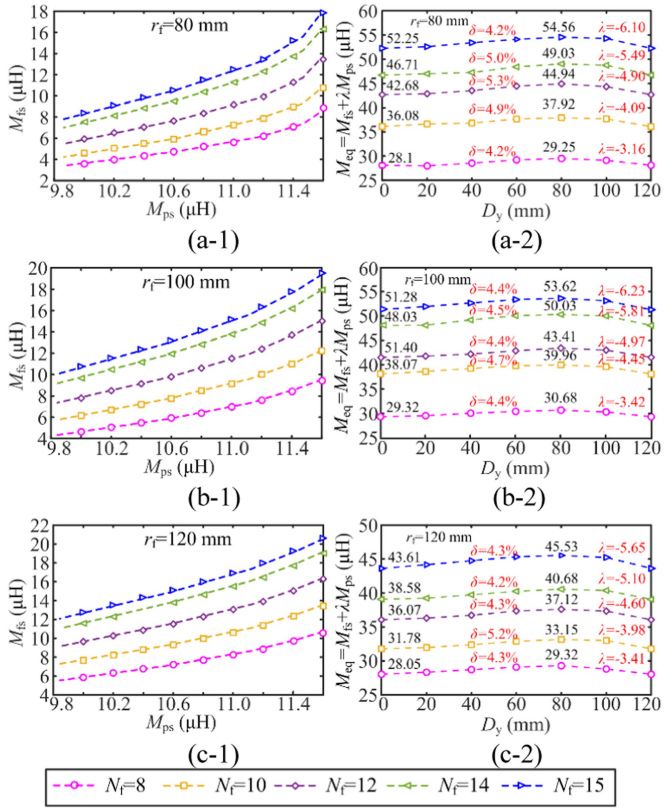

Fig. 4. Mutual inductances versus misalignment for different r_f and N_f. (a) $r_f = 80$ mm. (b) $r_f = 100$ mm. (c) $r_f = 120$ mm.

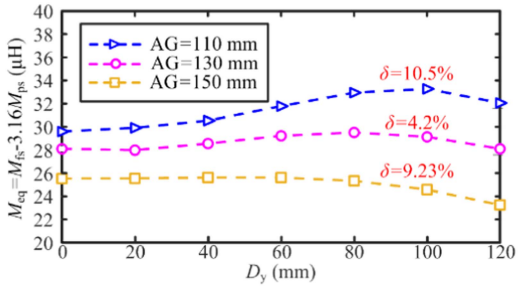

Fig. 5. Mutual inductances versus misalignment for different transfer distances.

region. This means the proposed system exhibits better misalignment tolerance. The value of the equivalent M_{eq} is magnified compared with the original M_{ps} and M_{fs}. Take $r_f = 80$ mm and $N_f = 8$ as an example, $M_{ps} = 11.72$ μH and $M_{fs} = 8.93$ μH when the misalignment distance $D_y = 0$ mm. Correspondingly, M_{eq} is 28.1 μH, which is much larger than M_{ps} and M_{fs}, even the sum ($M_{ps} + M_{fs} = 20.65$ μH), which contributes the efficient power transmission.

In the study, $r_f = 80$ with $Nf = 8$ is applied to analyze the performance of the proposed system considering the current stress [as shown in (8)] and the power loss. The corresponding λ is −3.16 and the M_{eq} fluctuation is 4.2%.

For different transmission distances AG, M_{eq} is compared in Fig. 5. It can be seen that the fluctuation δ of M_{eq} is about 10% within a transmission distance of [110 mm, 150 mm]. This means

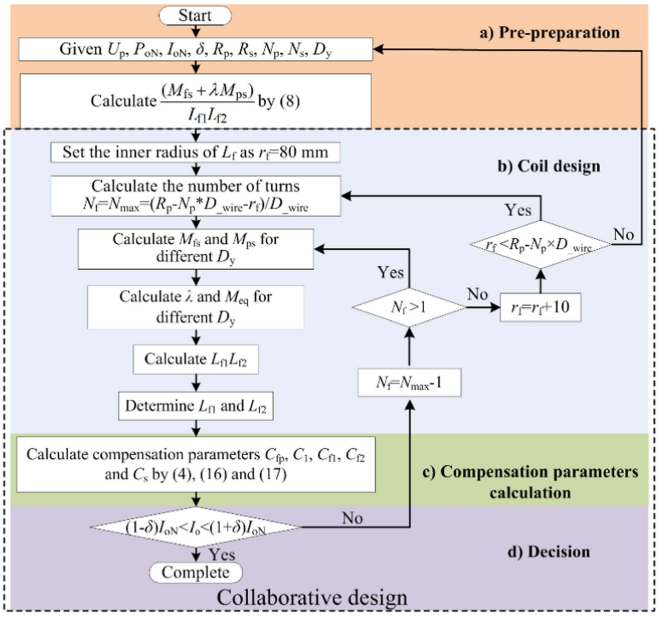

Fig. 6. Collaborative design flowchart.

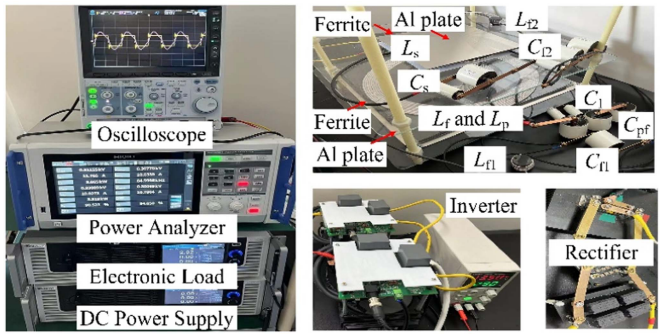

Fig. 7. Experimental setup.

TABLE II
PARAMETERS OF THE PROPOSED SYSTEM FOR EXPERIMENTAL

Parameter	Value	Parameter	Value	Parameter	Value
U_p	310 V	L_{f1}	64.85 μH	R_{Lf}	33.1 mΩ
f	85 kHz	L_{f2}	23.5 μH	R_{Lp}	108.7 mΩ
λ	-2.9	C_{f1}	60.81 nF	R_{Ls}	91.4 mΩ
L_f	36.8 μH	C_{f2}	157.4 nF	R_{Lf1}	46.6 mΩ
L_p	129.3 μH	C_1	11.29 nF	R_{Lf2}	18.35 mΩ
L_s	97.81 μH	C_{fp}	17.6 nF	R_L	10 Ω
M_{fp}	12.35 μH	C_s	45.43 nF	D_{wire}	5 mm

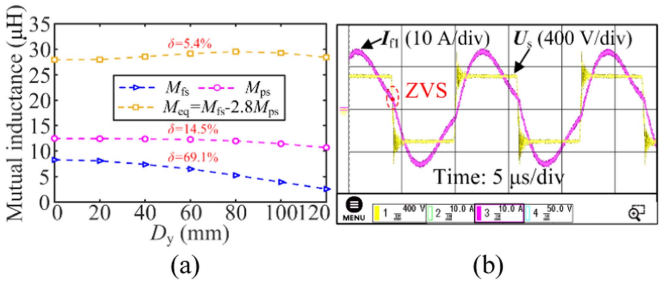

Fig. 8. Measured mutual inductances and inverter output. (a) Mutual inductances versus misalignment. (b) Output voltage and current of the inverter.

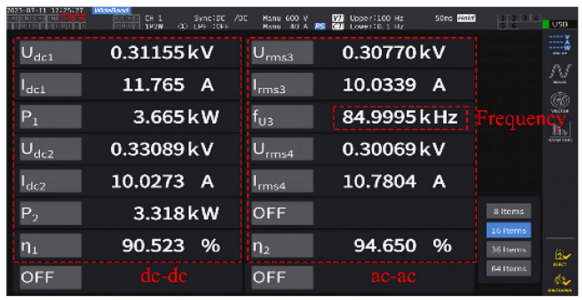

Fig. 9. Measured efficiency at the well-aligned position.

that the antioffset capability of the proposed system can also be maintained when the transfer distance changes in a certain range.

B. Collaborative Design of the Proposed System

The capacitor C_f can be calculated by using (7) and (13) as

$$C_f = \frac{1}{\omega^2 \left[L_f + KL_p - (K+1)M_{fp}\right]}. \tag{15}$$

The compensation capacitor C_{fp} is calculated by using (3), (6), (7), and (13) as

$$C_{fp} = \frac{1-K}{\omega^2 \left(M_{fp} - KL_p\right)}. \tag{16}$$

The compensation capacitor C_1 and C_{f1} can be calculated by using (1) and (15) and expressed as

$$\begin{cases} C_1 = \frac{C_f}{1-\omega^2 L_{f1} C_f} \\ C_{f1} = 1/\left(\omega^2 L_{f1}\right) \end{cases}. \tag{17}$$

Based on the abovementioned analysis, the design flowchart for the proposed dual-coupled system is shown in Fig. 6.

IV. Experimental Verification

For validation, a 3.3 kW with 10 A current prototype of the WPT system using the proposed method is built, as shown in Fig. 7. The design and measured parameters of the system are listed in Table II. The switch is VisIC 650V V22 GaN Transistor and the diode is DSEP2x31-06A.

For various misalignment distances, M_{ps} and M_{fs} are measured and then M_{eq} is calculated, as shown in Fig. 8(a). It can be seen that M_{eq} fluctuates slightly in the designed region and the value is 5.4%, which is much smaller than that of M_{fs} and M_{ps}. Notably, the value of M_{eq} is magnified from about 8.3 μH and 12.5 μH to 28 μH. The self-inductances Lf, Lp, and Ls are hardly changed with the mis-alignment, which is considered to be constant in the study. Fig. 8(b) shows the waveforms of inverter output $\boldsymbol{U}_s$ and $\boldsymbol{I}_{f1}$ with the well-aligned position. It can be seen that $\boldsymbol{I}_{f1}$ is always positive at the turn-OFF transition of MOSFETS and the phase of the inverter output current $\boldsymbol{I}_{f1}$ always remains lagging $\boldsymbol{U}_s$. Thus, ZVS can be obtained with the proposed method.

Fig. 9 shows the measured dc–dc efficiency and ac-ac efficiency at a well-aligned position. As shown in the figure, the

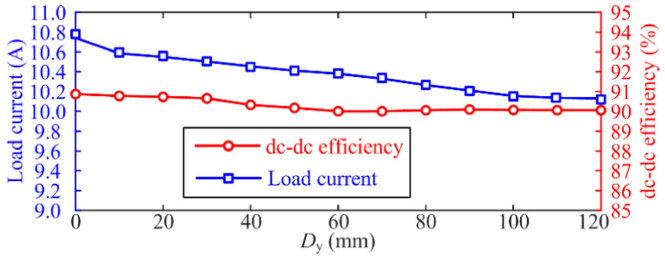

Fig. 10. Measured load current and efficiency for different misalignment distances.

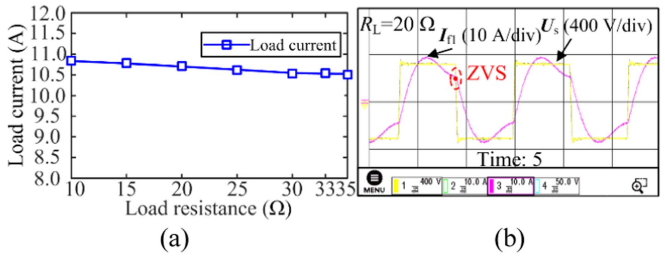

Fig. 11. Measured results for different load resistances. (a) Load current. (b) Inverter output for $R_L = 20\ \Omega$.

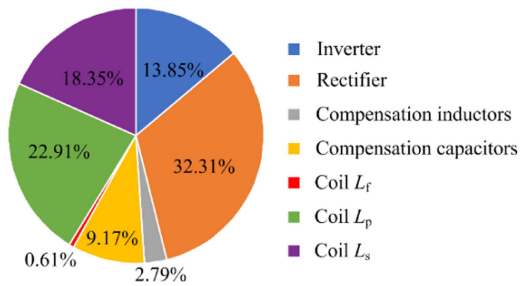

Fig. 12. Power loss distributions of each part.

ac–ac efficiency is 94.65% and the dc–dc efficiency is 90.523% when the output power is 3.318 kW. Notably, the inner resistance of the coils is larger due to the eddy effects of the Al plate, resulting in the efficiency decrease to a certain extent. The higher efficiency can be obtained when the Al plate is removed while the high misalignment is still maintained.

For various misalignment distances, the load current and the dc–dc efficiency are also measured and shown in Fig. 10. It can be seen that the load current can maintain stability with the misalignment and the maximum fluctuation is about 5%. Also, within the whole misalignment region, the dc–dc efficiency is stable and is maintained above 90%.

For different load resistances, the load current and the inverter output are measured, as shown in Fig. 11. It can be seen from Fig. 11(a) that the current changes from 10.91 A to 10.5 A as the load increases from 10 Ω to 35 Ω, which is 3.75% current variation under a relatively wide load change. In addition, ZVS can be also guaranteed when the load changes, as shown in Fig. 11(b).

The loss distribution of each part is shown in Fig. 12. The loss of the rectifier is the highest among all losses. It can be reduced by employing a synchronous rectifier circuit, which will be considered in the future.

TABLE III
COMPARISON OF REPORTED STUDIES AND PROPOSED SYSTEM

Ref.	[17]	[18]	[19]	This work
Coils	3 (Decoupled)	4 (Decoupled)	3	3
Al plate	No	No	No	Yes
P_{oN} (W)	300	200	~ 800	3300
Mis.	7.5% @D_x=90mm (AG=80mm)	5.8% @ D_x (D_y)=140mm (AG=100mm)	N/A @ D_x (D_y)=150mm (AG=120mm)	5% @ D_x (D_y)=120mm (AG=130mm)
$\eta_{dc\text{-}dc}$	93.56%	81.12%	~88 %	90.523%
ZVS	Yes	No	Yes	Yes
Output	Load dependent	CC	Load dependent	CC
MI	Maintain	Decreased	Maintain	Increased
Freedom	Low	Low	Medium	High

A comparison between the proposed dual-coupled system and the reported dual-coupled structures is shown in Table III, in which Mis. denotes the misalignment tolerance. Different from the other studies, the Al plate is applied in the letter, resulting in a slight decrease in the efficiency. The coils of the proposed system are not required decoupled and the design flexibility is improved. In addition, the stable magnified MI can be obtained with the proposed method and the efficient power is output stably. Also, ZVS input and load-independent CC output are guaranteed.

V CONCLUSION

To improve the anti-offset capability of WPT systems and the design flexibility of coils, an *LCCC-LCC* compensated dual-coupled WPT system is presented in this letter. Unlike the traditional antiseries coils, the restriction on the variation correlation of MI(s) is eliminated. Not only the similar transfer characteristic to that of the *LCC-LCC* compensated system, like the load-independent CC output with ZPA, but also the enhanced stable equivalent MI can be flexibly designed by introducing the MI adjustment factor. The experimental results validate the effectiveness of the proposed system.

REFERENCES

[1] S. Roy, A. N. M. W. Azad, S. Baidya, M. K. Alam, and F. Khan, "Powering solutions for biomedical sensors and implants inside the human body: A comprehensive review on energy harvesting units, energy storage, and wireless power transfer techniques," *IEEE Trans. Power Electron.*, vol. 37, no. 10, pp. 12237–12263, Oct. 2022, doi: 10.1109/TPEL.2022.3164890.

[2] Y. Liu, U. K. Madawala, R. Mai, and Z. He, "Zero-phase-angle controlled bidirectional wireless EV charging systems for large coil misalignments," *IEEE Trans. Power Electron.*, vol. 35, no. 5, pp. 5343–5353, May 2020, doi: 10.1109/TPEL.2019.2941709.

[3] Z. Luo, Y. Zhao, M. Xiong, X. Wei, and H. Dai, "A self-tuning LCC/LCC system based on switch-controlled capacitors for constant-power wireless electric vehicle charging," *IEEE Trans. Ind. Electron.*, vol. 70, no. 1, pp. 709–720, Jan. 2023, doi: 10.1109/TIE.2022.3153812.

[4] Y. Liu, U. K. Madawala, R. Mai, and Z. He, "An optimal multivariable control strategy for inductive power transfer systems to improve efficiency," *IEEE Trans. Power Electron.*, vol. 35, no. 9, pp. 8998–9010, Sep. 2020, doi: 10.1109/TPEL.2020.2970780.

[5] Y. Chen, R. Mai, Y. Zhang, M. Li, and Z. He, "Improving misalignment tolerance for IPT system using a third-coil," *IEEE Trans. Power Electron.*, vol. 34, no. 4, pp. 3009–3013, Apr. 2019, doi: 10.1109/TPEL.2018.2867919.

[6] P. Zhang, M. Saeedifard, O. C. Onar, Q. Yang, and C. Cai, "A field enhancement integration design featuring misalignment tolerance for wireless EV charging using LCL topology," *IEEE Trans. Ind. Electron.*, vol. 36, no. 4, pp. 3852–3867, Apr. 2021, doi: 10.1109/TPEL.2020.3021591.

[7] Y. Zhang, S. Chen, X. Li, and Y. Tang, "Design methodology of free-positioning non-overlapping wireless charging for consumer electronics based on antiparallel windings," *IEEE Trans. Ind. Electron.*, vol. 69, no. 1, pp. 825–834, Jan. 2022, doi: 10.1109/TIE.2020.3048322.

[8] W. Wang, C. Xu, C. Zhang, and J. Yang, "Optimization of transmitting coils based on uniform magnetic field for unmanned aerial vehicle wireless charging system," *IEEE Trans. Magn.*, vol. 27, no. 6, Jun. 2021, Art. no. 8600105, doi: 10.1109/TMAG.2021.3063796.

[9] Y. Chen et al., "Reconfigurable topology for IPT system maintaining stable transmission power over large coupling variation," *IEEE Trans. Power Electron.*, vol. 35, no. 5, pp. 4915–4924, May 2020, doi: 10.1109/TPEL.2019.2946778.

[10] Y. Zhang et al., "Misalignment-tolerant dual-transmitter electric vehicle wireless charging system with reconfigurable topologies," *IEEE Trans. Power Electron.*, vol. 37, no. 5, pp. 8816–8819, Aug. 2022, doi: 110.1109/TPEL.2022.3160868.

[11] L. Zhao, D. J. Thrimawithana, and U. K. Madawala, "A hybrid bidirectional IPT system with improved spatial tolerance," in *Proc. IEEE Int. Future Energy Electron. Conf.*, 2015, pp. 1–6, doi: 10.1109/IFEEC.2015.7361591.

[12] W. Zhao, X. Qu, J. Lian, and C. K. Tse, "A family of hybrid IPT couplers with high tolerance to pad misalignment," *IEEE Trans. Power Electron.*, vol. 37, no. 3, pp. 3617–3625, Mar. 2022, doi: 10.1109/TPEL.2021.3109639.

[13] P. Darvish, S. Mekhilef, and H. A. B. Illias, "A novel S–S–LCLCC compensation for three-coil WPT to improve misalignment and energy efficiency stiffness of wireless charging system," *IEEE Trans. Power Electron.*, vol. 36, no. 2, pp. 1341–1355, Feb. 2021, doi: 10.1109/TPEL.2020.3007832.

[14] S. Li, W. Li, J. Deng, T. D. Nguyen, and C. C. Mi, "A double-sided LCC compensation network and its tuning method for wireless power transfer," *IEEE Trans. Veh. Technol.*, vol. 64, no. 6, pp. 2261–2273, Jun. 2015, doi: 10.1109/TVT.2014.2347006.

[15] *SAE Wireless Power Transfer for Light-Duty Plug-In and Electric Vehicles and Alignment Methodology*, SAE Standard J2954, May 2019.

[16] X. Wang, L. He, J. Xu, and C. K. Lee, "Widening the operating range of a wireless charging system using tapped transmitter winding and bifrequency pulse train control," *IEEE Trans. Power Electron.*, vol. 37, no. 11, pp. 13874–13883, Nov. 2022, doi: 10.1109/TPEL.2022.3164465.

[17] Z. Yan et al., "Fault-tolerant wireless power transfer system with a dual-coupled LCC-S topology," *IEEE Trans. Veh. Technol.*, vol. 68, no. 12, pp. 11838–11846, Dec. 2019, doi: 10.1109/TVT.2019.2944841.

[18] Z. Yuan, M. Saeedifard, C. Cai, Q. Yang, P. Zhang, and H. Lin, "A misalignment tolerant design for a dual-coupled LCC-S-compensated WPT system with load-independent CC output," *IEEE Trans. Power Electron.*, vol. 37, no. 6, pp. 7480–7492, Jun. 2022, doi: 10.1109/TPEL.2022.3141453.

[19] Y. Wu, C. Liu, M. Zhou, X. Mao, and Y. Zhang, "An antioffset electric vehicle wireless charging system based on dual coupled antiparallel coils," *IEEE Trans. Power Electron.*, vol. 38, no. 5, pp. 5634–5637, May 2023, doi: 10.1109/TPEL.2023.3238353.